Optical properties of copper helical nanostructures: the effect of thickness on the SPR peak position

To cite this article: J Potonik *et al* 2022 *Nanotechnology* **33** 345710

IOP Publishing Nanotechnology
Nanotechnology 33 (2022) 345710 (11pp) https://doi.org/10.1088/1361-6528/ac705c

Optical properties of copper helical nanostructures: the effect of thickness on the SPR peak position

J Potočnik, N Božinović, M Novaković, T Barudžija, M Nenadović and M Popović

Vinča Institute of Nuclear Sciences—National Institute of the Republic of Serbia, University of Belgrade, Belgrade, Serbia

E-mail: jpotocnik@vinca.rs

Received 8 March 2022, revised 13 April 2022
Accepted for publication 17 May 2022
Published 7 June 2022

Abstract

In this study, we have investigated the effect of thickness on the structural and optical properties of copper (Cu) helical nanostructures. Thin films with thicknesses of 160 nm, 280 nm, 450 nm, and 780 nm were obtained by e-beam glancing angle deposition. The morphology and the microstructure were studied by field emission scanning electron microscopy, x-ray diffraction and transmission electron microscopy, while for the optical analysis measurements spectroscopic ellipsometry was used. The results show that the deposited structures are porous with nanometer-sized crystallites preferentially oriented along (111) planes, as well as that the diameter of the helices increases with thickness. Detailed analyses of optical properties have demonstrated that the dielectric function of Cu structures is greatly influenced by the films thicknesses. With increasing thickness from 160 nm to 780 nm, the surface plasmon resonance peak was shifted from 1.31 eV to 1.05 eV, which was correlated with the growth mechanism and the size of deposited nanostructures.

Keywords: copper, glancing angle deposition, helical nanostructures, ellipsometry, optical properties, surface plasmon resonance

(Some figures may appear in colour only in the online journal)

1. Introduction

In recent years, scientists and researchers have been focused on obtaining and characterizing thin films in order to explain the film formation, growth mechanisms, and their special structural properties. Thin film structure is influenced by the type of the substrate, the film thickness as well as the deposition parameters, which determine their physical properties [1]. In this sense, microstructural characterization (grain size, defect density, texture, etc) is essential for understanding the deposition processes and deposition conditions and, finally, their effect on the properties of thin films [2, 3].

Synthesis of different thin films can take place through a variety of deposition techniques. The examples of the most commonly used methods are molecular beam epitaxy (MBE) [4], e-beam evaporation technique [5], pulsed laser deposition [6], sol-gel technique [7], chemical vapor deposition methods (CVD) [8, 9], or different sputtering techniques (DC or RF sputtering) [10]. In recent years, however, considerable attention has been devoted to the development of the methods dealing with formation of specific nanostructures, such as nanocrystalline silicon (nc-Si), nanostructured TiO_2, carbon nanotubes (CNTs), graphene, ZnO nanoparticles (NPs), etc. For instance, Sharma *et al* [5] have used e-beam evaporation assisted physical vapor deposition (EBPVD) for the formation of nc-Si films, and have shown that this technique is more convenient for the deposition of nanocrystalline films rather than conventional plasma enhanced CVD method (PECVD). On the other side, due to the specific application demands, in the case of carbon nanotubes deposition, in particular for vertically aligned CNTs, the researchers mostly prefer CVD techniques, like PECVD or floating catalyst CVD (FCCVD) method [9, 11]. Moreover, Zhang *et al* [12] have shown that copper nanostructures in the form of high-density nanowires uniformly distributed in a narrow

space (pores) could be obtained via metal organic chemical vapor deposition (MOCVD). Nonetheless, when the formation of specific 3D columnar nanostructures is required, e-beam glancing angle deposition (GLAD) is widely used. Since the deposition is performed at an oblique angle, the shadowing effect is very important for acquiring specific structures. When the vapor atoms nucleate on the substrate, the regions behind each grain cannot receive more atoms, thus resulting in a porous film with isolated columns. Glancing angle deposition has been used for obtaining a variety of nanostructures such as pillars, slanted columns, zigzag structures and helices [13]. Due to their unique physical and chemical properties [14], this type of metallic nanostructures has found wide application in different technological fields such as electronics [15], reflection [16], plasmonics [17–22], catalysis [23, 24], mechanics [25], etc.

Copper has been investigated for many years because of its characteristic physical properties, such as low electrical resistivity, high thermal conductivity and low resistivity coefficient [26–28]. Due to these properties, Cu has found use in electronic industry, wireless communications, as conducting material in integrated circuits, etc. In particular, nanostructured Cu films possess distinctive mechanical, thermal, magnetic, electric and catalytic properties, which make them suitable for application in many fields such as industry, medicine, and the environment [29]. Furthermore, Cu thin films could be used in solar cells [30], diodes [31], catalysis [32], high-speed integrated circuits [33, 34], sensors [35], fungicidal and nematicidal applications [36–38], etc. The grain size control of nanostructured Cu thin films and its effect on physical properties are very important for electronic applications [39], since the deposition process of semiconductors determines the grain size-band gap dependence [40]. Aside from grain size, the overall microstructure has a significant impact on the electrical conductivity of Cu thin films [41, 42].

The main goal of this research was to study the structural and optical properties of helical Cu thin films obtained by e-beam glancing angle deposition. The effects of thickness on the characteristics of the samples are discussed on the basis of grain size and diameter of the columns, and also on the films porosity induced by the shadowing effect. Field emission scanning electron microscopy (FESEM), x-ray diffraction (XRD) and conventional and high-resolution transmission electron microscopy (TEM/HRTEM) have been used to analyze the morphological and crystallographic structure of the helical Cu films. For the investigation of optical properties of the thin films, in particular for the analysis of surface plasmon resonance (SPR) effect, spectroscopic ellipsometry measurements were performed. The obtained results indicate that the observed structural and optical properties differ for various structures, being dependent on the film thickness. Specifically, the changes are related to the different diameters of the Cu helices, which are in turn defined by dissimilar growth mechanisms during the films deposition processing.

2. Materials and methods

Copper (Cu) thin films were deposited from Cu metallic target purity of 99.999% (Onyx Met) in a home-made deposition chamber at the base pressure of 8×10^{-5} Pa before each run, while the pressure during deposition was approximately 2×10^{-4} Pa. The emission current of 180 mA and voltage of 1.8 kV were used for Cu evaporation. During the deposition, two step-motors were used: the first one was employed for the adjustments of the deposition angle, and the second one for the substrate rotations. The substrates used were single-crystalline (100) silicon wafers which were ultrasonically cleaned with ethanol, distilled and deionized water. They were positioned at the distance of 25 cm from the copper target surface, and were oriented in such way that the deposition angle was 85°. In order to obtain nanostructures with a helical shape, during the deposition process, the substrates were slowly rotated around the normal axis, with 5° step and the rotation speed of 0.03 rpm. Cu films were deposited with the growth rate of approximately 2 nm min^{-1} to the thickness of 160 nm, 280 nm, 450 nm and 780 nm, as monitored by a quartz crystal placed into the deposition chamber.

The morphology and thickness of the deposited Cu thin films were analyzed by field emission scanning electron microscopy (FESEM) using FEI SCIOS 2, Dual Beam electron microscope, operated at 20 kV. Planar view FESEM micrographs were also employed to determine the porosity of copper thin films, utilizing ImageJ software [43]. The crystallographic structure, including the orientation and size of Cu crystallites, was examined by x-ray diffraction technique. XRD patterns were obtained by PHILIPS 1050 x-ray diffractometer using Ni-filtered Cu-K$\alpha_{1,2}$ radiation and Bragg-Brentano focusing geometry. The measurements were taken in the 25°–65° 2θ range, with the step size of 0.05° and a counting time of 5 s per step. The analysis of diffraction lines and determination of the crystallite size was carried out by using Topas software package [44]. In order to investigate structure of the thin films more detailed, cross-section lamellas of the samples were prepared by focus ion beam (FIB) and observed by conventional and high-resolution transmission electron microscopy (TEM/HRTEM), on 200 kV FEI Talos F200X microscope. An energy dispersive x-ray spectroscopy (EDS) system attached to the TEM, operating in scanning transmission (STEM) mode, was used for spatially-resolved EDS analysis. The optical properties of Cu samples were investigated by spectroscopic ellipsometry measurements. The spectra were collected by Jobin-Yvon UVISEL 5 spectroscopic ellipsometer operating in the energy range from 0.6 eV to 4.8 eV with a step of 0.1 eV, at an incidence angle of 70°. Data acquisition and modeling of the obtained results were carried out using DeltaPsi2 software [45].

3. Results and discussion

The structure and the morphology of deposited Cu films were analyzed by field emission scanning electron microscopy. In figure 1 are given FESEM micrographs of Cu nanostructures, taken in cross-sectional (left side) and in the planar view (right side). According to the cross-sectional images, the thickness of the deposited samples was verified and

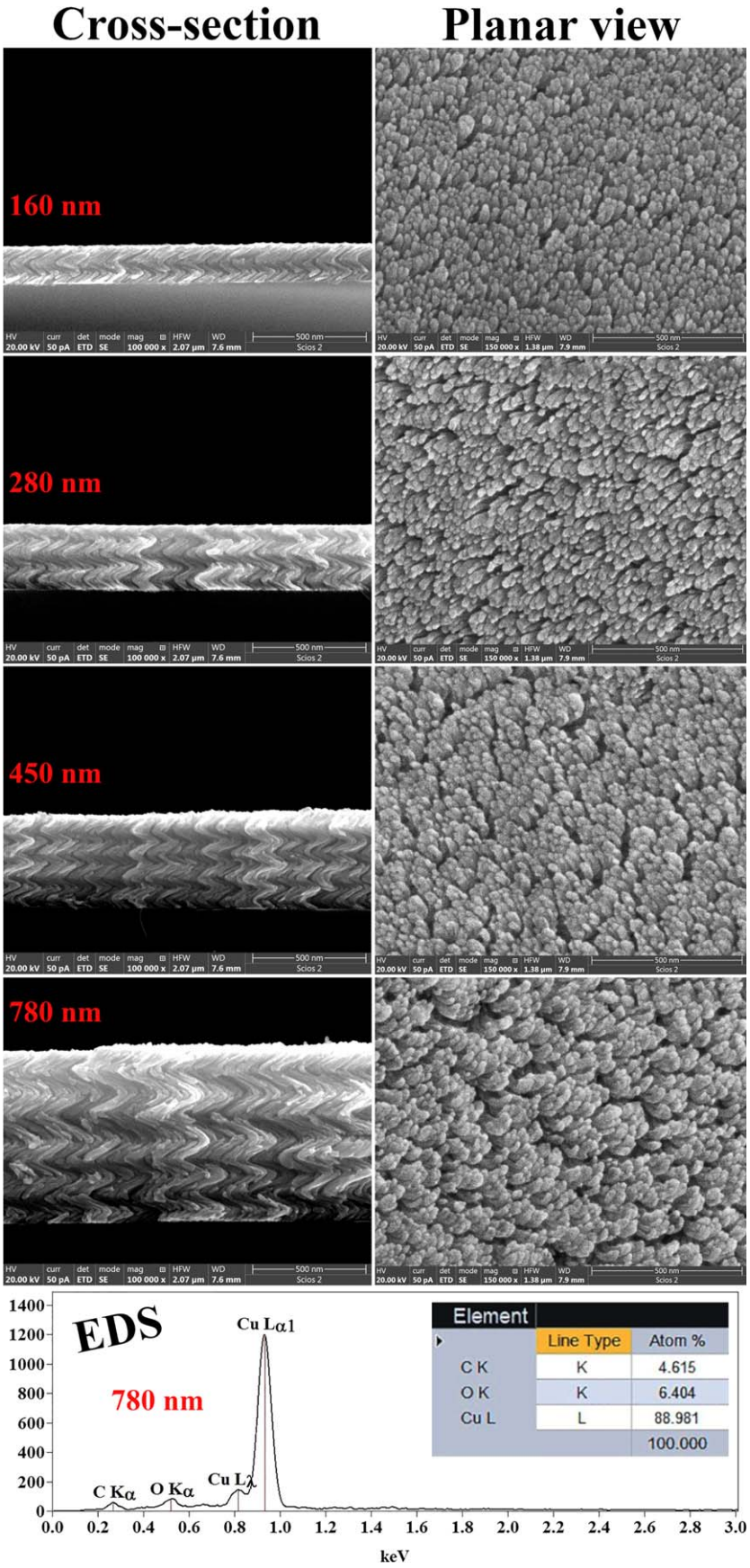

Figure 1. FESEM micrographs of helical Cu nanostructures with different thicknesses (160 nm, 280 nm, 450 nm and 780 nm): cross-sectional view (left side) and planar view (right side). EDS spectrum of 780 nm thick Cu film is presented in the bottom of the image. Scale bars correspond to different magnifications: 100 kx for cross-sectional view and 150 kx for planar view.

determined as 160 nm, 280 nm, 450 nm and 780 nm. It is clearly visible that the deposited nanostructures have a helical shape, as well as that the helices are uniformly distributed through the sample and become well-defined with increasing film thickness. Also, it can be seen that the length and diameter of the helices are approximately constant from the substrate to the surface within each sample. By detailed observation of the planar view micrographs, it can be noticed that the diameters of the helices increase with film thickness, where the roughly estimated values found to be up to a few tens of nanometers. The obtained helical nanostructures are formed by slow rotation of the substrate with respect to the surface normal, as compared to the deposition rate. In this way, the growth direction of the thin films also rotates, i.e. the incident vapor direction changes, as well as the direction of the column growth, and the obtained structures are spiraling upwards from the substrate [46]. Thus, the structure of the formed helices could be controlled through the substrate rotation, by controlling the time interval between each rotation step, and also by the deposition angle. With these parameters, one can control the diameter of the helices, as well as their length [47].

In order to analyze and check the chemical composition of the samples, EDS analysis was also performed and the typical EDS spectrum, collected for the 780 nm thick film in the energy range of 0.1–5 keV, is presented in figure 1 (the range from 0.1–3 keV is given for clarity). The most intense peak seen below 1.5 keV belongs to copper (Cu Lα_1), and next to it is a smaller one that refers to the Cu Lλ line. Two peaks, positioned at lower energies, are associated with oxygen (O Kα) and carbon (C Kα). The existence of oxygen is probably due to the oxidation of copper, will be discussed later in the text, while the presence of carbon could be associated with the impurities adsorbed on the sample surface.

Another important observation seen from FESEM micrographs is a porosity of deposited films, coming from the shadowing effect which occurs during the GLAD deposition [46]. It can be seen that the films become more porous with increasing thickness, which is especially noticeable in the micrographs taken in planar view. This is expected because the deposition process takes place in such way that the incoming vapor atoms arrive at the substrate at a certain angle and quickly physisorbed on the surface, forming nuclei of different sizes on it. As the nuclei grow and form nanocolumns, more atoms are deposited on them and at that point some smaller columns remain shadowed by the larger ones and their growth stops. In this way, porous microstructures develop continuously during the deposition of thin films on the basis of shadowing effect and competitive growth [46].

Based on the FESEM micrographs, presented in figure 1, we were able to calculate the porosity of Cu thin films using computing software ImageJ [43]. A description of the image analysis procedure, as well as the achieved results are depicted in figure 2. FESEM micrograph, obtained for 160 nm Cu sample, is displayed in figure 2(a), whereas figure 2(b) shows the grey level histogram that was used to separate the phases. To estimate the quantity of porosity, the threshold is set to the default in order to separate the pores from the matrix of the sample. When the threshold is set, the pores were highlighted in red, as can be seen in figure 2(c). After ensuring that just the pores are marked in red, the examination can continue to produce a binary image with segregated porosity (figure 2(d)). Finally, the 'analyze particles' option was chosen to acquire pore area data. As a result, the rough regions of the sample surface are represented in white, while pores are presented in black color. The analysis was also performed for 280 nm, 450 nm and 780 nm copper samples and the results showed that the porosity increases with film thickness and equals to the values of 31%, 35%, 42% and 48%.

Phase analyses of the helical Cu thin films were carried out with XRD. The results are presented in figure 3, showing x-ray diffraction patterns of the Cu films together with a simulated diffractogram of Cu phase. The analysis confirms that the Cu phase with the face-centered cubic structure is formed during the deposition, as verified by the existence of the peaks at $2\theta = 43.33°$ and $2\theta = 50.44°$, which belong to (111) and (200) characteristic reflections of copper (PDF No. 01-089-2838), respectively. It can be seen in all cases that the (111) reflection is well-defined with the intensity much stronger than that of (200) line. In order to determine whether the preferential crystallite orientation was present, the experimental patterns were compared with a simulated one of Cu phase that was calculated by assuming random orientation of the crystallites. The intensity ratios of the (111) and (200) peaks indicate that the preferential orientation of Cu crystallites is along (111) plane. Also, one notices that overall peaks become more intense when increasing thickness, thus indicating the improvement of the films crystallinity. Another important characteristic of the spectra is that apart from the peaks corresponding to (111) and (200) reflections of Cu, we observe two weak peaks at the angles $2\theta = 36.44°$ and $2\theta = 61.89°$. Since these peaks exactly match the position of (111) and (200) reflections of Cu_2O (PDF No. 01-077-0199) this is an indication of the presence of metal-oxide phase in the films. Indeed, this is in agreement with the results of EDS analysis (see figure 1), according to which the existence of oxygen in the deposited structures was confirmed. Based on the results, we assume that the part of copper was probably oxidized during the deposition process due to the increasing the diameter of Cu helices and surface coverage. This explanation supports the fact that the intensity of Cu_2O peaks increases with the increase of the film thickness. Nonetheless, this phenomenon can also be result of spontaneous surface oxidation as a consequence of high surface/volume ratio after the samples were removed from the deposition chamber and exposed to air, as already reported in the literature [48].

Another parameter obtained from XRD spectra is the grain size of the copper crystallites for different Cu samples. The mean grain size was calculated using Topas software [44], which applies the fundamental parameters approach to the line profile fitting. The size of Cu crystallites was found to be between 8 nm and 10 nm, as the thickness of the samples increases from 160 nm to 780 nm, while the Cu_2O crystallites are found to be smaller, ranging in size from 4 nm to 7 nm.

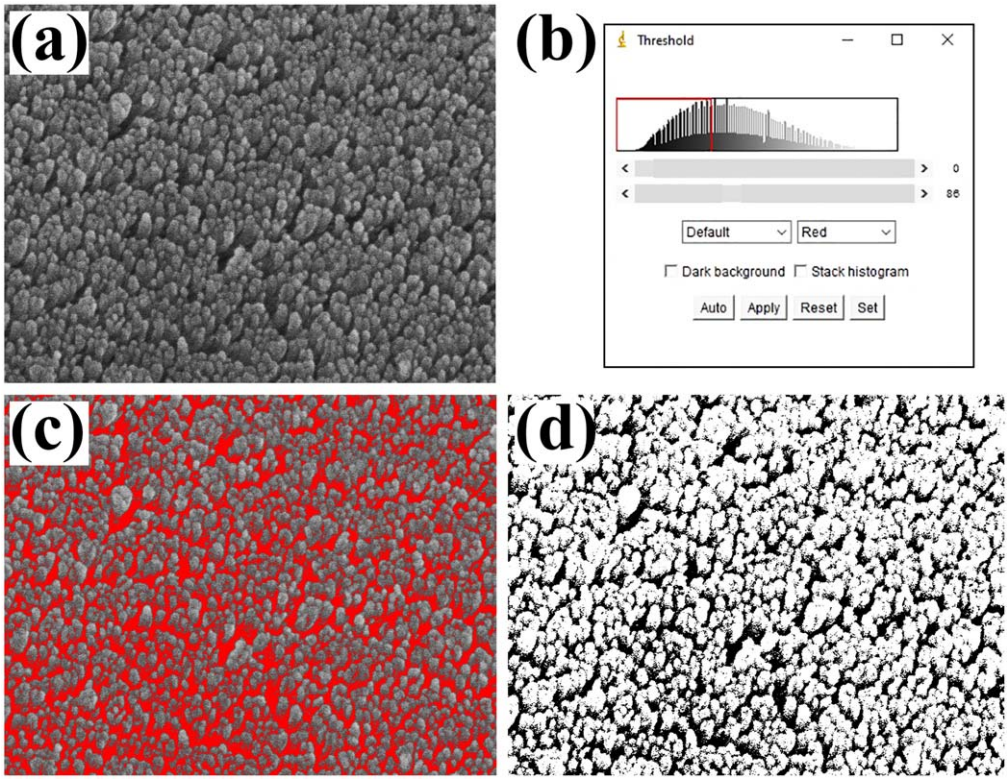

Figure 2. Description of the ImageJ software analysis procedure on the basis of 160 nm Cu thin film: (a) original FESEM micrograph, (b) analogous grey level histogram, (c) analyzed picture and (d) binary image of 160 nm copper sample.

This practically means that under given deposition conditions, films with fine-grained structure were produced.

In order to obtain detailed information on the microstructure of different Cu films and also to establish the exact size of helices diameters, the samples were analyzed by cross-sectional transmission electron microscopy. As an example, figure 4 presents low (a), (d) and high (b), (e) magnification TEM micrographs, and corresponding HRTEM images (c), (f), for the two selected samples thicknesses of 160 nm and 780 nm, respectively. Low magnification micrographs of both samples show general microstructure with helical-shaped Cu films formed onto the Si substrate, covered by Pt overlayer, which was used as protective layer during the FIB preparation of TEM lamellas. Based on the presented images it is obvious that the samples exhibit different thicknesses, but regardless to the duration of films deposition processes similar morphologies are formed. This means that Cu helical structures on silicon substrates follow a general similar behavior which can be obtained via GLAD processing. Indeed, the microstructure is more clearly visible in high magnification images, presented in figures 4(b) and (e). As can be seen in both cases the helix diameters and also the spacing between adjacent helices appear to be fairly constant along the growing film, starting from the bottom up to the sample surface. A closer examination, however, shows that depending on the thickness of nanostructures the diameters of the individual helices differ; in particular, we found it increases with film thickness (note that the scale bars in the presented TEM micrographs correspond to different image magnifications). An average value of diameter for the film with the thickness of 160 nm found to be 10 nm, while it is even twice as larger in the case of 780 nm thick sample, where the diameters of 20 nm were measured. The structure of the samples was further analyzed at higher magnifications and the HRTEM micrographs of isolated helices were also presented for both samples (figures 4(c) and (f)). The micrographs confirm crystalline structure of the films, showing well-defined lattice planes. The measured interplanar spacing of 0.208 nm and 0.209 nm is in a very good agreement with the theoretical value for (111) planes of cubic Cu. Apart from this, HRTEM micrographs show the presence of Cu_2O (111) planes with *d*-spacing of 0.245 nm. The presence of oxygen was also confirmed by EDS elemental color mapping analysis. Figure 5 presents STEM/HAADF micrograph of the 780 nm thick Cu film with corresponding image maps, where different colors were associated with different elements. The yellow, red, green and cyan color micrographs correspond to oxygen, copper, platinum and silicon, respectively. Based on the images it is evident that the Cu and O elements are evenly distributed over the deposited film.

Analysis of the optical properties of helical Cu nanostructures was carried out by spectroscopic ellipsometry. This surface-sensitive technique directly gives two experimental parameters, ellipsometric angles Ψ and Δ, which are related to the ratio of reflection coefficients for light polarized parallel and perpendicular to the plane of incidence, respectively [49]. Typical (Ψ, Δ) spectra taken from different Cu samples are presented in figure 6. The interpretation of the obtained results

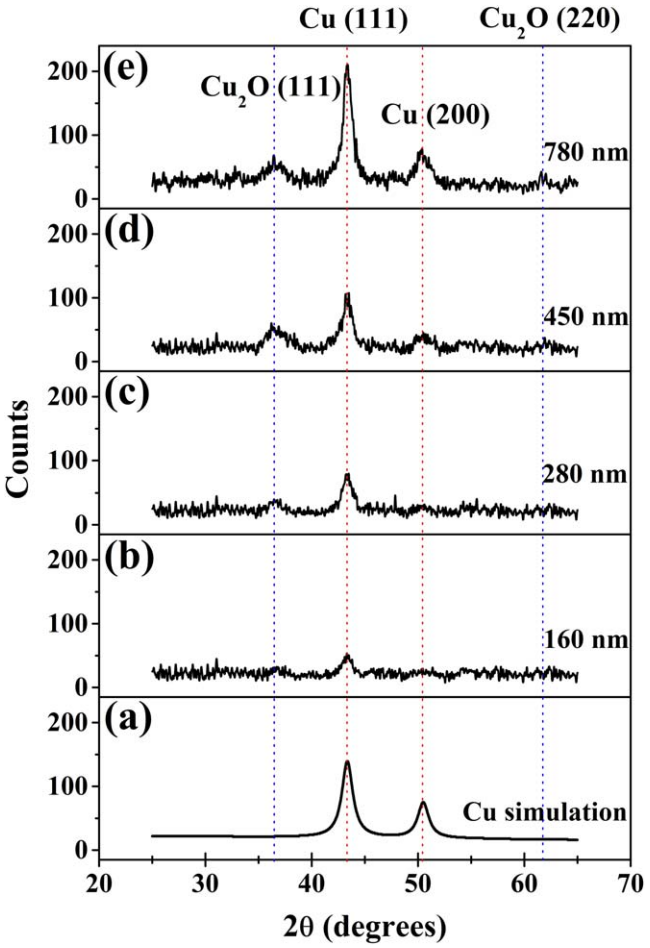

Figure 3. Simulated XRD spectrum of Cu phase (a) and the patterns of Cu nanostructures thicknesses of 160 nm (b), 280 nm (c), 450 nm (d) and 780 nm (e).

from the absolute (Ψ, Δ) values is difficult because the change in polarization does not contain any readily useful information. The extraction of meaningful physical data requires construction of an appropriate model, where each layer refers to a given material, and the calculated data must be fitted to the experimental ones. In order to utilize spectroscopic ellipsometry analysis more accurately, it is necessary to have knowledge on the films structure. For this matter, we have used FESEM micrographs to get values of the thicknesses of the layers, which were incorporated into the optical model and presumed constant during the fitting. Since copper thin films are considered as inhomogeneous, this non-uniformity was simulated by the use of different concentrations of voids in the deposited layers. By additional analysis we found that the inclusion of the surface roughness in the model improved the quality of the fit, by reducing the mean squared error, known as chi-square (χ^2), which quantifies the 'goodness' of the fit. Based on this, a roughness layer was also included in the optical model and was allowed to vary in the range from 1 nm to 10 nm (note that the void fraction, i.e. the volume fraction of air in this layer was kept constant). During the fitting procedures the quantity χ^2 was always below 3, thus meaning the used model may be considered to be correct.

For the modelling of Cu nanostructures, we assume four-layer system (schematically presented as the inset in figure 6(a)): one layer containing Cu together with Cu_2O and voids, then silicon substrate as an underlying layer which consists of crystalline silicon with the native oxide layer on the top. An additional layer was used to describe the roughness of the films, presenting a discrete layer that contains a mixture of the copper oxide with voids in a 50:50 ratio using an effective medium approximation (EMA). The film structure for all samples was fitted with Drude–Tauc Lorenz model, where Drude term describes the metallic character of the system due to intraband transitions, while Tauc-Lorentz dispersion formula is related to the interband transitions of the valence electrons. Thus, the dielectric function for the helical Cu nanostructures could be described using the sum of two terms:

$$\varepsilon = \varepsilon_D + \varepsilon_{TL} \tag{1}$$

in which the first term represents Drude, while the second describes Tauc-Lorentz dielectric functions. Drude dielectric function is given by [50]:

$$\varepsilon_D = \varepsilon_\infty - \frac{\omega_p^2}{-\omega^2 + i\Gamma_d\omega}, \tag{2}$$

where ε_∞ is the high-frequency contribution, ω_p is plasma frequency and Γ_d is the damping factor. While the ε_D illustrates the metallic nature of Cu, the second term in equation (1) was used to model SPR contributions using Tauc-Lorentz dispersion law as follows [51]:

$$\varepsilon_r = \varepsilon_{r,\infty} + \frac{2}{\pi} \cdot P\int_{E_g}^{\infty} \frac{\xi \cdot \varepsilon_i(\xi)}{\xi^2 - E^2} d\xi \tag{3}$$

and

$$\varepsilon_i = \frac{1}{E} \cdot \frac{AE_0 \cdot C(E - E_g)^2}{(E^2 - E_0^2)^2 + C^2 \cdot E^2}. \tag{4}$$

Equations (3) and (4) define real and imaginary parts of the dielectric function, respectively, where $\varepsilon_{r,\infty}$ presents high-frequency dielectric constant, E_g optical band gap, E photon energy, E_0 peak central energy, C broadening term of the peak and A Tauc-Lorentz coefficient.

Based on the ellipsometric fitting data the porosities of the deposited Cu nanostructures were obtained. The results showed that, as the thickness grows from 160 nm to 780 nm, the obtained values for porosity are (32 ± 3)%, (37 ± 3)%, (44 ± 4)%, (51 ± 5)%, indicating that the acquired results are in good agreement with those derived from FESEM micrographs using ImageJ software. Since during the GLAD processing, the formation of specific nanostructures is caused by the shadowing effect, with increasing thin film thickness the columns become thicker and thus affects the formation of larger voids between them. In this way, the porosity of the deposited thin films increases as well. The obtained results could be related with those found from EDS and XRD measurements, where in the case of thick samples the larger amount of oxygen was observed. Indeed, higher porosities provide pronounced surface-to-volume ratios, thus enabling the amount of oxygen increases with respect to the thickness.

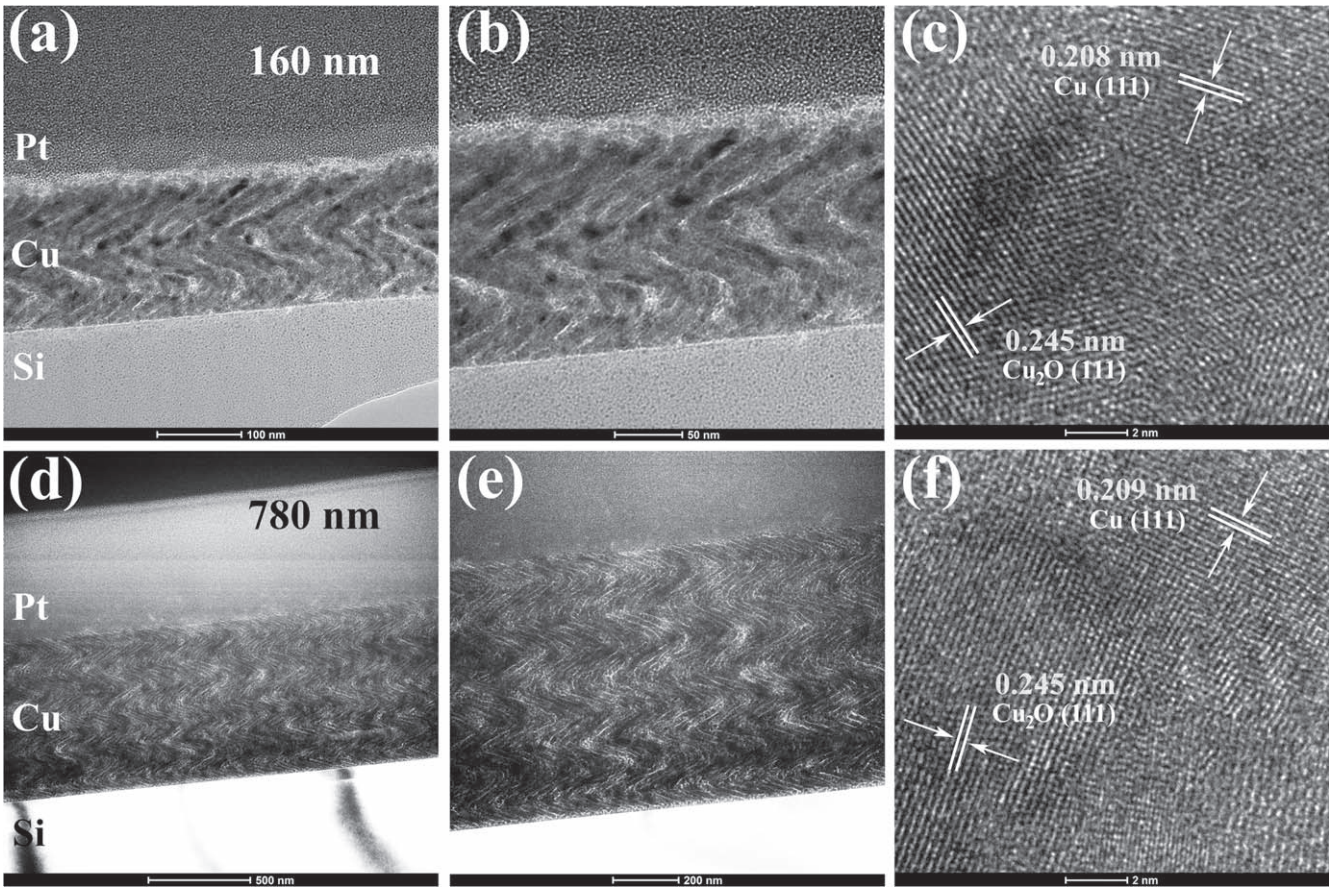

Figure 4. TEM analysis of Cu helical nanostructures deposited onto Si substrates: low magnification (a), (d), high magnification (b), (e) and HRTEM (c), (f) micrographs of 160 nm and 780 nm thick samples, respectively. Scale bars correspond to different magnifications: 100 nm (a), 50 nm (b), 2 nm (c), 500 nm (d), 200 nm (e) and 2 nm (f).

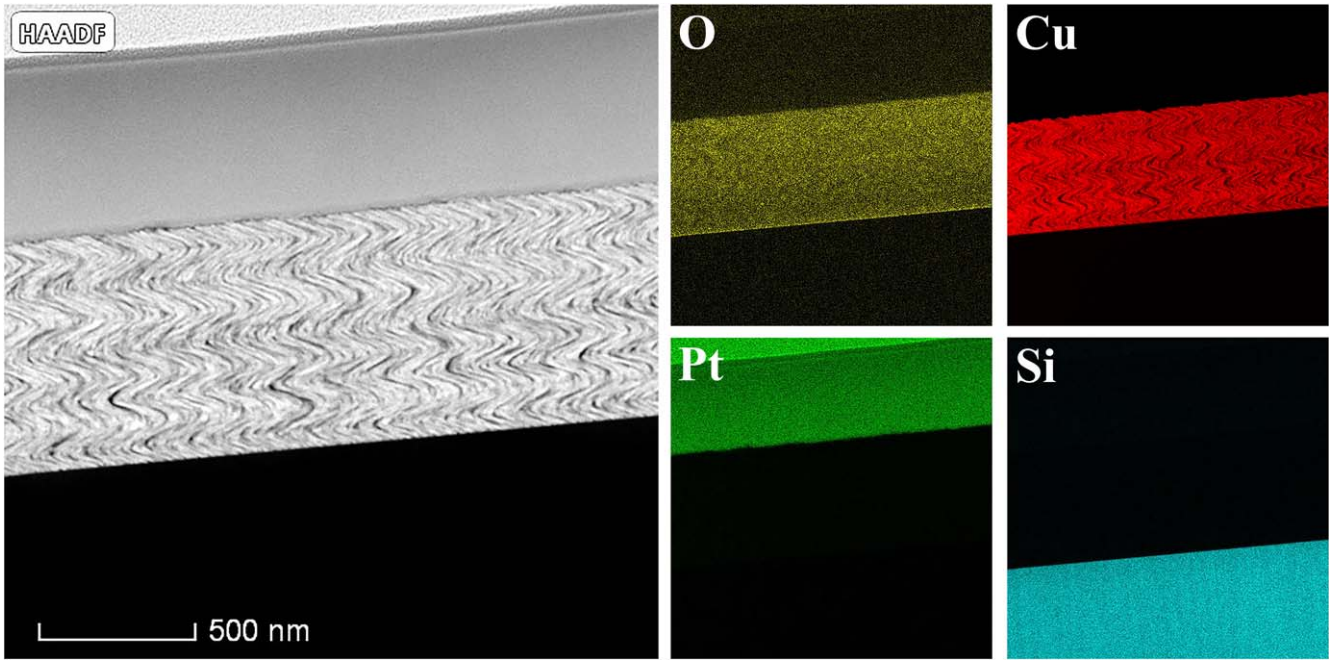

Figure 5. STEM/HAADF image with corresponding EDS maps highlighting the O, Cu, Pt and Si elements for 780 nm thick Cu film deposited onto Si substrate. Pt overlayer was used as a protective layer during the FIB preparation of TEM lamella.

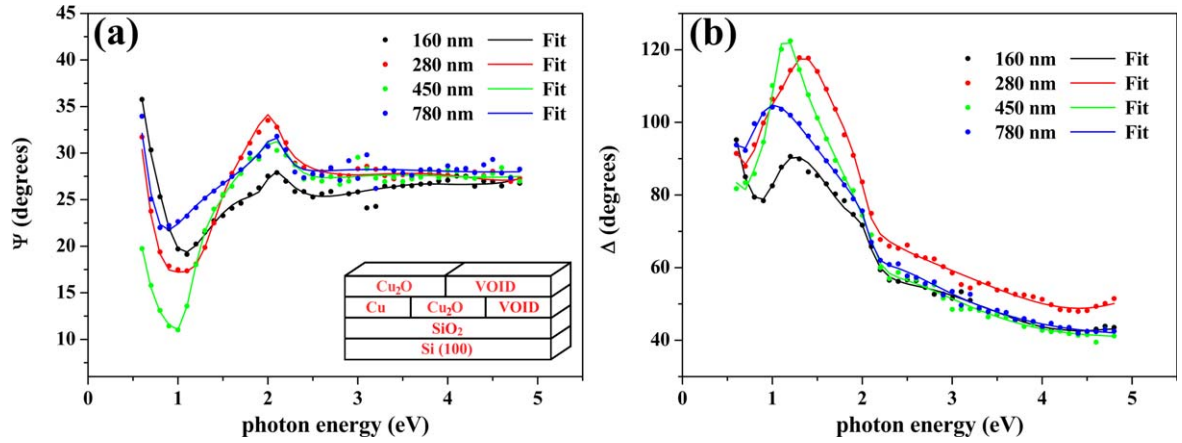

Figure 6. Experimental (geometric symbols) and fitted data (solid lines) of ellipsometric parameters (a) Ψ and (b) Δ for the helical Cu thin films with different thicknesses, as a function of photon energy. The optical model of copper, used to analyze the spectroscopic ellipsometry data, is schematically presented in the inset of figure (a).

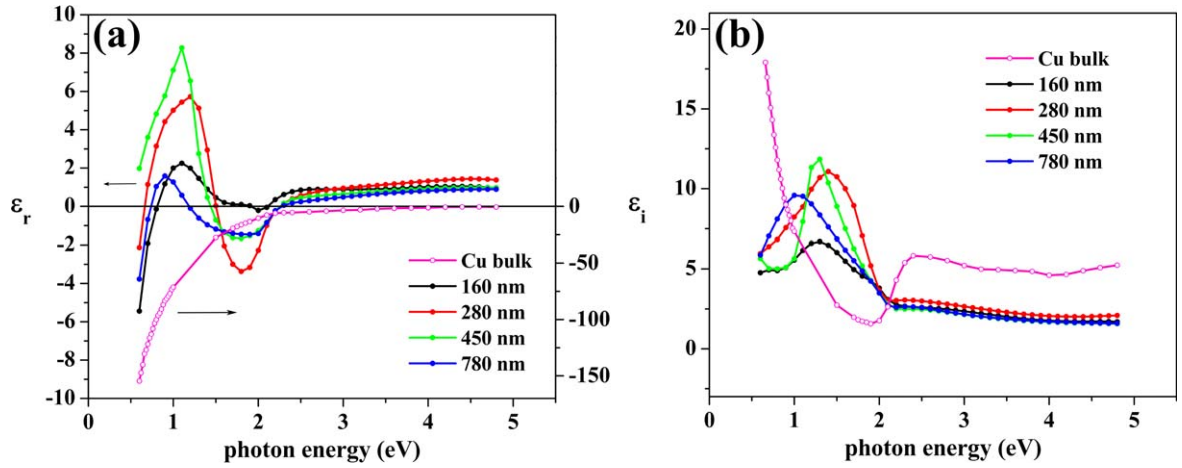

Figure 7. Real (ε_r) and imaginary (ε_i) parts of the dielectric function for Cu bulk, 160 nm, 280 nm, 450 nm and 780 nm thick nanostructured Cu films determined from ellipsometry measurements. Data for Cu bulk are taken from the literature.

In addition, modeling of the measured parameters (Ψ, Δ) enabled determination of the complex dielectric function ($\varepsilon = \varepsilon_r + \varepsilon_i$), which is correlated with the nanostructure and electronic structure of the Cu films. The real (ε_r) and imaginary (ε_i) parts of complex dielectric function for all Cu samples are plotted in figure 7. For comparison with the optical response of deposited copper thin films, the spectra for bulk Cu, taken from literature [52], were also presented in the figure. The ε_r spectra are of particular interest here since they are considered to be characteristic of the chemical and structural quality of the films. As can be seen for nanostructured Cu samples, the photon energy range from 1.2 eV to 2.3 eV (figure 7(a)) is characterized by negative values of ε_r, which come from the interaction of light with conduction electrons [53], thus reflecting the metallic character of the deposited structures [54]. However, contrary to the bulk Cu, which is characterized by negative ε_r in whole spectral range, Cu films display a band between 0.7 eV and 1.9 eV, where ε_r exhibits positive values. This practically means that the films did not retain a metallic response, confirming non-Drude behavior in this spectral region, which differs significantly from copper's optical behavior [55]. Similar findings, however, were observed previously, where the appearance of this band has been related to the formation of either cuprous (Cu_2O) or cupric (CuO) oxide depending on the conditions leading to the oxide formation [56, 57]. Indeed, this is in agreement with the microstructural and chemical analyses done by XRD and HRTEM, where the presence of Cu_2O phase was confirmed. Finally, the real part of the dielectric function also displays positive values for photon energies above 2.3 eV. The positive values of ε_r in this part of the spectrum are expected since they come from the damping oscillations due to the collisions of the electrons to the nucleus. Overall, the magnitude of ε_r varied with thickness typically from 160 to 450 nm. As seen from the spectra in figure 7(a), there are differences in the nature for the 780 nm thick layer stemming possibly from differences in thickness, structure and composition.

Apart from the real parts of dielectric functions of Cu nanostructures, the imaginary parts ε_i should be also considered, since they present contribution of different energy losses in the material. The ε_i spectra for Cu films, as well as for bulk Cu, are presented in figure 7(b), as a function of photon energy of the incident light. As it can be seen, all spectra obtained for copper nanostructures display a clearly visible absorption peak at the photon energies below 2 eV, whereas at the energies above 2 eV

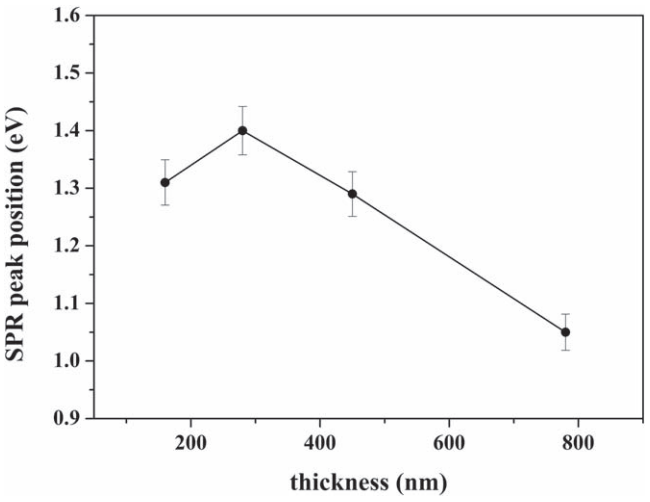

Figure 8. Dependence of the SPR peaks position on the thickness of the deposited Cu thin films.

no significant absorption is observed. The presence of these peaks could be associated to an appearance of the SPR absorption of Cu nanoparticles representing collective oscillations of conduction electrons. These oscillations occur as a result of the interaction between the electroactive radiation and metal nanostructures [58]. However, by comparing spectra for bulk Cu and nanostructured copper thin films it can be seen that the SPR peaks for thin films are shifted toward lower photon energies (for bulk Cu SPR peak is at 2.4 eV). The existence of SPR absorption was found earlier by other authors [59–61] for plasmonic copper nanoparticles synthesized by different deposition methods. Although, it should be mentioned that Cu helices obtained here exhibit absorption at much lower photon energy values, located in the IR part of the spectrum, as compared to those found in the literature. This difference could come from the changes in the shape and size of the diameter of the nanostructures, as well as growth mechanism (island-like growth) [62] and the dielectric properties of the environment [63]. Besides, the development and the shift of the absorption band could be also accompanied with the Cu oxidation [57] and formation of Cu_2O phase. In addition, one also observes change in the position of SPR peaks, as to the difference in the thickness of Cu nanostructures. Typically, with increasing film thickness, SPR peak exhibit a red shift, as shown in figure 8. For example, SPR peak is centered at 1.31 eV for the Cu film with the thickness of 160 nm, while for the 780 nm thick sample it is positioned at the 1.05 eV. The SPR peak is not only shifted to lower photon energies, but with changing films thickness displays difference in width and intensity as well. The observed changes are most likely the result of wide distribution of size of Cu particles and strong contribution of their agglomerations. In particular, the observed bands are broad due to the agglomeration of nanoparticles in the samples [64].

4. Conclusions

Helical Cu thin films were deposited by e-beam GLAD to the thicknesses in the range of 160–780 nm. Optical properties of Cu helices were investigated and correlated with the thickness of the films, and therefore with their microstructure. The obtained results reveal that the deposited films are porous and both structural and optical properties of the films are strongly affected by the thickness of the samples. According to XRD and TEM measurements, it was found that besides metallic Cu, there is a certain amount of Cu_2O in the deposited samples. Also, TEM analysis showed that with increasing the film thickness from 160 nm to 780 nm the diameter of nanostructures also increases from 10 nm to 20 nm. As to the optical properties, i.e. the dielectric functions of the films, they are found to be determined by the thickness and the microstructure of the deposited thin films, but also by the Cu oxidation and formation of Cu_2O phase. Generally, SPR peak follows a red shift from 1.31 eV to 1.05 eV with increasing the films thickness from 160 nm to 780 nm. The SPR peak is not only shifted to lower photon energies, but also displays a difference in width and intensity. It is assumed that overall changes in SPR position are due to wide distribution of sizes of Cu particles and the strong contribution of their agglomerations, which is a consequence of the changes in the sample thickness. On the basis of the presented results, it can be concluded that glancing angle deposition enables the formation of specific Cu nanostructures with highly tunable SPRs, thus making them very attractive candidates for plasmonic applications.

Acknowledgments

This research was funded by the Ministry of Education, Science and Technological Development of the Republic of Serbia.

Data availability statement

All data that support the findings of this study are included within the article (and any supplementary files).

ORCID iDs

J Potočnik https://orcid.org/0000-0001-7206-5952
N Božinović https://orcid.org/0000-0002-4762-4115
T Barudžija https://orcid.org/0000-0002-9240-9609

References

[1] Hojabri A, Hajakbari F, Moghri Moazzen M A and Kadkhodaei S 2012 Effect of thickness on properties of copper thin films growth on glass by DC planar magnetron sputtering *J. Nanostruct.* **2** 107–12
[2] Knorr D B and Lu T M 1991 Effects of deposition conditions on texture in copper thin films on Si (111) *Textures Microstruct.* **13** 155–64
[3] Tracy D P and Knorr D B 1993 Texture and microstructure of thin copper films *J. Electron. Mater.* **22** 611–6

[4] Schumann T, Goyal M, Kim H and Stemmer S 2016 Molecular beam epitaxy of Cd3As2 on a III–V substrate *APL Mater.* **4** 126110

[5] Sharma P, Tripathi N and Gupta N 2017 Nanocrystalline silicon thin film prepared by e-beam evaporation for display application *J. Mater. Sci., Mater. Electron.* **28** 3891–6

[6] Dolbec R, Khakani M A, Serventi A M, Trudeau M and Saint-Jacques R G 2002 Microstructure and physical properties of nanostructured tin oxide thin films grown by means of pulsed laser deposition *Thin Solid Films* **419** 230–6

[7] Dutta M, Mridha S and Basak D 2008 Effect of sol concentration on the properties of ZnO thin films prepared by sol–gel technique *Appl. Surf. Sci.* **254** 2743–7

[8] Sharma P, Pavelyev V, Kumar S, Mishra P, Islam S S and Tripathi N 2020 Analysis on the synthesis of vertically aligned carbon nanotubes: growth mechanism and techniques *J. Mater. Sci., Mater. Electron.* **31** 4399–443

[9] Hofmann S, Ducati C, Robertson J and Kleinsorge B 2003 Low-temperature growth of carbon nanotubes by plasma-enhanced chemical vapor deposition *Appl. Phys. Lett.* **83** 135–7

[10] Soderberg H, Oden M, Molina-Aldareguia J M and Hultman L 2005 Nanostructure formation during deposition of TiN/SiNx nanomultilayer films by reactive dual magnetron sputtering *J. Appl. Phys.* **97** 114327

[11] Hou P X, Zhang F, Zhang L, Liu C and Cheng H M 2022 Synthesis of carbon nanotubes by floating catalyst chemical vapor deposition and their applications *Adv. Funct. Mater.* **32** 2108541

[12] Zhang Y, Lam F L-Y, Hu X, Yan Z and Sheng P 2007 Fabrication of copper nanowire encapsulated in the pore channels of SBA-15 by metal organic chemical vapor deposition *J. Phys. Chem.* C **111** 12536–41

[13] He Y and Zhao Y 2011 Advanced multi-component nanostructures designed by dynamic shadowing growth *Nanoscale* **3** 2361–75

[14] Liu L, Zhang L, Kimb S M and Park S 2014 Helical metallic micro- and nanostructures: fabrication and application *Nanoscale* **6** 9355–65

[15] Kosugi T 2013 Electronic properties and persistent spin currents of nanospring under static magnetic field *J. Phys. Soc. Jpn.* **82** 034703

[16] Lu Z, Zhao M, Xie P, Wu L, Yu Y, Zhang P and Yang Z 2012 Reflection properties of metallic helical metamaterials *J. Lightwave Technol.* **30** 3050–4

[17] Fan Z and Govorov A O 2012 Chiral nanocrystals: plasmonic spectra and circular dichroism *Nano Lett.* **12** 3283–9

[18] Ziegler J and Haglund R 2013 Complex polarization response in plasmonic nanospirals *Plasmonics* **8** 571–9

[19] Li Y R, Ho R M and Hung Y C 2013 Plasmon hybridization and dipolar interaction on the resonances of helix metamaterials *IEEE Photonics J.* **5** 2700510

[20] Zhang Z Y and Zhao Y P 2008 Optical properties of helical and multiring Ag nanostructures: the effect of pitch height *J. Appl. Phys.* **104** 013517

[21] Zhang Z Y and Zhao Y P 2007 Optical properties of helical Ag nanostructures calculated by discrete dipole approximation method *Appl. Phys. Lett.* **90** 221501

[22] Trevino J, Cao H and Dal Negro L 2011 Circularly symmetric light scattering from nanoplasmonic spirals *Nano Lett.* **11** 2008–16

[23] An W, Pei Y and Zeng X C 2008 CO oxidation catalyzed by single-walled helical gold nanotube *Nano Lett.* **8** 195–202

[24] Yang J, Li B, Zhang Q, Yim W and Chen L 2012 Catalytic oxygen activation on helical gold nanowires *J. Phys. Chem.* C **116** 11189–94

[25] da Fonseca A F and Galvao D S 2004 Mechanical properties of nanosprings *Phys. Rev. Lett.* **92** 175502

[26] Edelstein D C, Sai-Halasz G A and Mii Y J 1995 VLSI on-chip interconnection performance simulations and measurements *IBM J. Res. Dev.* **39** 383–401

[27] Pai P L and Ting C H 1989 Copper as the future interconnection materials *Proc. of the 6th Int. IEEE VLSI Multilevel Interconnection Conf.* pp 258–64

[28] Murarka S P 1997 Multilevel interconnections for ULSI and GSI era *Mater. Sci. Eng.* **R19** 87–151

[29] Lee B, Kim Y, Yang S, Jeong I and Moon J 2009 A low-cure-temperature copper nano ink for highly conductive printed electrodes *Curr. Appl. Phys.* **9** e157–60

[30] Fthenakis V M and Kim H C 2007 Cu(InGa)Se2 thin-film solar cells: comparative life-cycle analysis of buffer layers *22nd European Photovoltaic Solar Energy Conf.* p 5

[31] Nienhaus H, Bergh H S, Gergen B, Majumdar A, Weinberg W H and McFarland E W 1999 Ultrathin Cu films on Si(111): Schottky barrier formation and sensor applications *J. Vac. Sci. Technol.* **A17** 1683

[32] Ponce A A and Klabunde K J 2005 Chemical and catalytic activity of copper nanoparticles prepared via metal vapor synthesis *J. Mol. Catal. A* **225** 1–6

[33] Kim K J, Kim J H and Kang J H 2001 Structural and optical characterization of Cu_3N films prepared by reactive RF magnetron sputtering *J. Cryst. Growth* **222** 767–72

[34] Cale T S, Merchant T P, Borucki L J and Labun A H 2000 Topography simulation for the virtual wafer fab *Thin Solid Films* **365** 152–75

[35] Xu Q, Zhao Y, Xu J Z and Zhu J J 2006 Preparation of functionalized copper nanoparticles and fabrication of a glucose sensor *Sensors Actuators* B **114** 379–86

[36] Mohamed E A, Gaber M H and Elsharabasy S F 2018 Evaluating the *in vivo* efficacy of copper-chitosan nanocomposition for treating vascular wilt disease in date palm *Int. J. Environ., Agric. Biotechnol.* **3** 447–54

[37] Mohamed E A 2018 Non-dependency of *in vitro* fungicidal efficiency of copper nanoparticles against fusarium oxysporum upon particle size *J. Plant Pathol. Microbiol.* **9** 432

[38] Mohamed E A, Elsharabasy S F and Abdulsamad D 2019 Evaluation of *in vitro* nematicidal efficiency of copper nanoparticles against root-knot nematode meloidogyne incognita *South Asian J. Parasitol.* **2** 1–6

[39] Vopsaroiu M, Thwaitesa M J, Fernandez G V, Lepadatu S and O'Grady K 2005 Grain size effects in metallic thin films prepared using a new sputtering technology *J. Optoelectron. Adv. Mater.* **7** 2713–20

[40] Tyagi P and Vedeshwar A G 2001 Grain size dependent optical band gap of CdI_2 films *Bull. Mater. Sci.* **24** 297–300

[41] Aithal R K, Yenamandra S, Gunasekaran R A, Coane P and Varahramyan K 2006 Electroless copper deposition on silicon with titanium seed layer *Mater. Chem. Phys.* **98** 95–102

[42] Ho C-E, Chen C-C, Lu M-K, Lee Y-W and Wu Y-S 2016 *In-situ* study on the self-annealing behavior of electroplated Cu through the cantilever method, XRD, and EBSD *Surf. Coat. Technol.* **303** 86–93

[43] National Institute of Health, USA, https://rsb.info.nih.gov/ij/

[44] Cheary R W, Coelho A A and Cline J P 2004 Fundamental parameters line profile fitting in laboratory diffractometers *J. Res. Nat. Inst. Stand. Technol.* **109** 1–25

[45] Horiba Scientific, DeltaPsi2 Software, https://www.horiba.com/int/products/detail/action/show/Product/deltapsi2-software-1648/

[46] Hawkeye M M, Taschuk M T and Brett M J 2014 *Glancing Angle Deposition of Thin Films: Engineering the Nanoscale* (New York: Wiley)

[47] Zhao Y P, Ye D X, Wang G C and Lu T M 2003 Designing nanostructures by glancing angle deposition *Proc. SPIE* **5219** 59–73

[48] Santos A J, Lacroix B, Maudet F, Corvisier A, Paumier F, Dupeyrat C, Girardeau T, García R and Morales F M 2019 Surface oxidation of amorphous Si and Ge slanted columnar and mesoporous thin films: evidence, scrutiny and limitations for infrared optics *Appl. Surf. Sci.* **493** 807–17
[49] Haidu F, Gordan O D and Zahn D R T 2012 In sity ellipsometric study of copper growth on silicon *Thin Solid Films* **520** 4410–7
[50] Rosenberg H M 1988 *The Solid State* (Oxford: Oxford University Press)
[51] Jellison G E and Modine F A 1996 Parameterization of the optical functions of amorphous materials in the interband region *Appl. Phys. Lett.* **69** 371–4
[52] Palik E D 1985 *Handbook of Optical Constants of Solids* vol I (New York: Academic)
[53] Popović M, Novaković M, Schmidt E, Schoppe P, Bibić N, Ronning C and Rakočević Z 2017 Low-loss and tunable near-zero-epsilon titanium nitride *Opt. Mater.* **72** 775–80
[54] Novaković M, Popović M, Rakočević Z and Bibić N 2017 Structural, optical and electrical properties of reactively sputtered Cr_xN_y films: nitrogen influence on the phase formation *Process. Appl. Ceram.* **11** 45–51
[55] Oates T W H, Wormeester H and Arwin H 2011 Characetrization of plasmonic effect in thin films and metamaterials using spectroscopic ellipsometry *Prog. Surf. Sci.* **86** 328–76
[56] Tahir D and Tougaard S 2012 Electronic and optical properties of Cu, CuO and Cu_2O studied by electron spectroscopy *J. Phys.: Condens. Matter* **24** 175002
[57] Fabijanić I, Janicki V, Ferre-Borrull J, Bubaš M, Blažek Bregović V, Marsal L F and Sancho-Parramon J 2019 Plasmonic nanoparticles and islands films for solar energy harvesting: a comparative study of Cu, Al, Ag and Au performance *Coatings* **9** 382
[58] Ghosh S K and Pal T 2007 Interparticle coupling effect on the surface plasmon resonance of gold nanoparticles: from theory to applications *Chem. Rev.* **107** 4797–862
[59] Mohamed E A 2020 Green synthesis of copper and copper oxide nanoparticles using the extract of seedless dates *Heliyon* **6** e03123
[60] Kaminskiene Ž, Prosyčevas I, Stonkute J and Guobiene A 2013 Evaluation of optical properties of Ag, Cu and Co nanoparticles synthesized in organic medium *Acta Phys. Pol.* A **123** 111–4
[61] Al-Haddad R M S, Ibrahim I M and Khalid A H 2014 The study of the nonlinear optical properties of copper nanoparticles prepared by pulse laser ablation PLA *Int. J. Eng. Res. Appl.* **4** 89–96
[62] Doremus R H 1966 Optical properties of thin metallic films in island form *J. Appl. Phys.* **37** 2775
[63] Kelly K L, Coronado E, Zhao L L and Schatz G C 2003 The optical properties of metal nanoparticles: the influence of size, shape and dielectric environment *J. Phys. Chem.* B **107** 668
[64] Ghodselahi T, Vesaghi M A and Shafiekhani A 2009 Study of surface plasmon resonance of $Cu@Cu_2O$ core–shell nanoparticles by Mie theory *J. Phys. D: Appl. Phys.* **42** 015308